Editors' Suggestion

Temperature Rise Associated with Adiabatic Shear Band: Causality Clarified

Yazhou Guo,[1,2,3] Qichao Ruan,[1,2,3] Shengxin Zhu,[4,6] Q. Wei,[1,5] Haosen Chen,[4,6,*] Jianan Lu,[1,2,3] Bo Hu,[1,2,3] Xihui Wu,[1,2,3] Yulong Li,[1,2,3,†] and Daining Fang[4,‡]

[1]*School of Aeronautics, Northwestern Polytechnical University, Xi'an 710072, China*
[2]*Shaanxi Key Laboratory of Impact Dynamics and Engineering Application, Northwestern Polytechnical University, Xi'an 710072, China*
[3]*Joint International Research Laboratory of Impact Dynamics and Engineering Application, Northwestern Polytechnical University, Xi'an 710072, China*
[4]*Institute of Advanced Structure Technology, Beijing Institute of Technology, 100081, Beijing, China*
[5]*Department of Mechanical Engineering, University of North Carolina at Charlotte, Charlotte, North Carolina 28223, USA*
[6]*State Key Laboratory of Explosion Science and Technology, Beijing Institute of Technology, Beijing 100081, China*

(Received 21 August 2018; published 10 January 2019)

One of the most important issues related to adiabatic shear failure is the correlation among temperature elevation, adiabatic shear band (ASB) formation and the loss of load capacity of the material. Our experimental results show direct evidence that ASB forms several microseconds after stress collapse and temperature rise reaches its maximum about 30 μs after ASB formation. This observation indicates that temperature rise cannot be the cause of ASB. Rather, it might be the result of adiabatic shear localization. As such, the traditional well-accepted thermal-softening mechanism of ASB needs to be reconsidered.

DOI: 10.1103/PhysRevLett.122.015503

Adiabatic shear band (ASB), first observed by Tresca in 1878, is considered one of the most important failure mechanisms of materials under impact loading [1]. ASB is usually described as having a very large shear strain (10^0–10^2) that occurs in a narrow (10^0–10^2 μm) nearly planar region of the material within an extremely short amount of time (10^0–10^2 μs), accompanied by severe local temperature rises (as high as 10^3 K) [2]. In fact, early studies of ASB since its discovery by Tresca did not gain much progress until 1944 when Zener and Hollomon interpreted ASL as a physical process of thermal-plastic instability [3]. They, and many other scholars following them, believed that ASB initiation is the result of competition between thermal softening and strain or strain-rate hardening [4–12]. Based on this assumption, temperature-induced material attenuation was always adopted as the initial weakening in most physical and mathematical classical analyses of ASL. What is more, experimental evidences such as recrystallization within ASBs also point to temperature rise during ASB [13–20]. This naturally led to the thesis that temperature rise is fundamentally the cause of ASB. Such a thesis constitutes the foundation of most efforts related to ASB and has been commonly accepted by the mainstream researchers in the community. However, according to the best knowledge of the present authors, this important notion has not been subject to direct experimental examinations. Mechanistic models based on this notion often lead to unrealistic predictions that cannot be experimentally validated. For example, the well-known model of critical shear strain for ASB initiation by Culver [12] is $\gamma_c = [(n\rho c_V)/\alpha]$, where ρ is the density, c_V the specific heat, n the strain hardening exponent, and $\alpha = [(\partial\tau)/(\partial T)]$ the thermal softening rate, respectively. This equation indicates that γ_c should vanish if $n = 0$. However, recent experimental observations indicate that γ_c is very large or even no ASB comes into being for some ultrafine-grained or nanostructured metals [21–23] whose n is zero or even negative under compressive loading.

In fact, many researchers tried to clarify the role of thermal softening in the process of ASL by determining the temperature rise itself. One indirect but popular method is estimating the temperature rise via work-heat conversion [24–28]. Its accuracy, however, relies on the choice of the conversion coefficient (or the Taylor-Quinney factor) which in itself is an issue of great controversy [29,30]. The direct *in situ* experimental measurements of temperature rise in relation to shear band evolution are rather difficult due to the *transient* and *local* nature of ASB. The first attempt to measure the temperature of a propagating shear band was made by Costin *et al.* [31] who measured the average temperature of a spot containing a shear band by a high-speed single-element infrared (IR) InSb (indium antimonide) detector. After that, Duffy and co-workers [32–35], Ranc *et al.* [36], and Rittel *et al.* [19,37,38] performed a series of tests on the ASL behavior of metals, including temperature rise within ASB. Although their results vary greatly, the temperature elevation is confirmed and found to be from a few hundred to above 1000 K. However, all this experimental evidence seems to have shown that temperature rise and ASB formation occur simultaneously

(or *almost* simultaneously), but they did not provide clear evidence of their causal relationship.

In this Letter, we try to clarify the causality of temperature rise and ASB using a Kolsky bar [or split Hopkinson pressure bar (SHPB)] synchronized with a high-speed photographic system and an IR temperature measurement system. The roles of impact loading, deformation, and temperature pertinent to the ASL process could be intuitively identified by comparing the sequence of important observations such as stress drop, strain localization, temperature rise, ASB initiation, and so on. Recent advancement of high-speed photography enables us to acquire high resolution deformation fields around ASB.

Shear tests were conducted using an SHPB apparatus that has been articulated and now widely used for dynamic compression. The working principles and technical details of SHPB can be found elsewhere [39]. Shear-compression specimen (SCS) which is similar to what is used by Rittel *et al.* [19,40] is adopted. Grid lines were carved on the surface of the specimen's gauge section to display the deformation clearly. The test material in this work is commercial titanium with grade II purity. The composition of the material is (all in wt %) 0.08 Fe, 0.01 C, 0.009 N, 0.008 H, 0.1 O, and balance Ti.

The temperature measurement system includes an optical system with 1:1 magnification and an eight-channel IR detector. The detector is made of InSb that responds to radiation in the 1 to 5.5 μm wavelength range corresponding to temperature from 60 °C to 1200 °C, which is adequate for measuring shear band temperatures. The response time for the detector is less than 1 μs, fast enough for SHPB tests. Each of the elements in the detector array is a 0.15×0.15 mm square. The separation between two adjacent elements is 50 μm. The deformation process of the specimen is recorded by a high-speed camera with the highest framing rate of 5×10^6 frames/sec. The flash, camera, and IR system are all triggered by the incident pulse of the stress wave. The time sequence for each device can be easily derived by calculating the time period during which the loading pulse travels from the incident strain gauge to the specimen. Calibration of the IR system is of vital importance to the reliability and accuracy of temperature measurement. A relationship between temperature and voltage needs to be established before the actual test. In the present work, each of the eight elements are individually calibrated.

Thirty dynamic tests with IR temperature measurements were conducted in this work, among which eight tests were equipped with synchronized high-speed photography. The shear stress and temperature evolution with respect to time are presented in Fig. 1. The deformation of the shear-compression specimen could be divided into three stages, i.e., (i) uniform deformation, (ii) nonuniform deformation, and (iii) shear localization. The characteristics of deformation at these different stages are given in Fig. 2. Severe

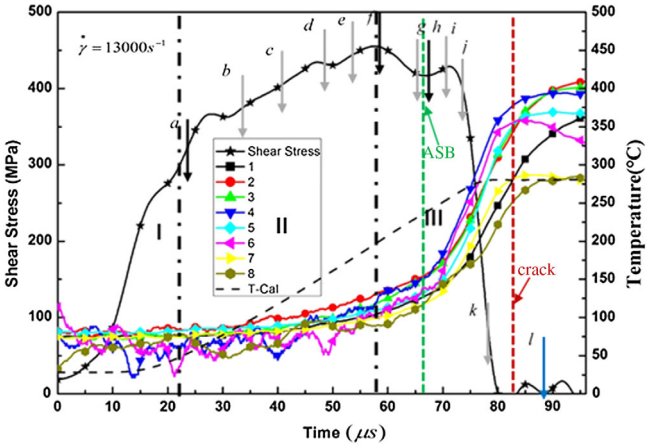

FIG. 1. Deformation history of a shear-compression specimen, showing the time, shear stress, and temperature. Numbers in the boxed legend indicate the eight detectors (or locations) where temperatures are measured. The three stages (I, II, and III) are marked by vertical dotted lines. The arrows $a - l$ correspond to the times at which the high-speed photographing system captures snapshots of the specimen. Four representative snapshots of the specimen are shown in Fig. 2 that correspond to the times of a, f, h, and l in Fig. 1. T-Cal, the dashed line, is the calculated temperature based on the conversion of mechanical work to heat (taking 1.0 as the Taylor-Quinney factor). The dashed green and red lines denote the appearances of ASB and crack, respectively.

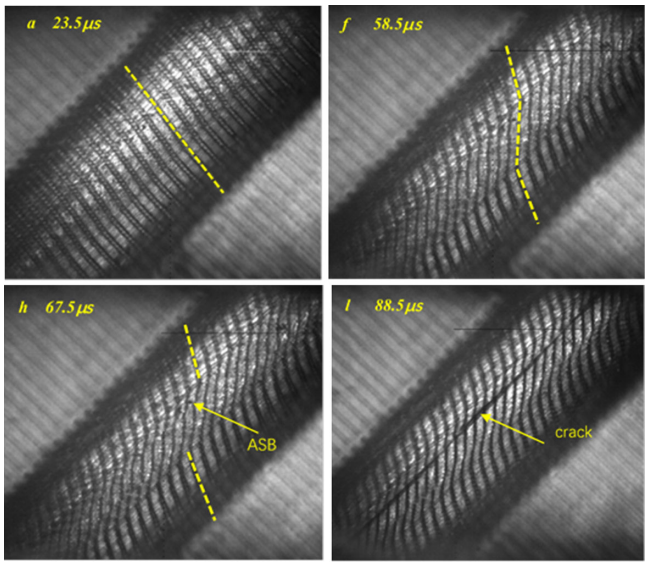

FIG. 2. Four representative high-speed photographic snapshots to show the deformation of a shear-compression specimen under dynamic loading. The letter at the upper left corner of each snapshot correpsonds to the time of Fig. 1. (a) Before any plastic deformation; (f) Uniform deformation at the peak stress or immediately before softening; (h) Adiabatic shear band—deformation is now highly localized, contrasting (f); (l) presents a crack as a consequence of the ASB.

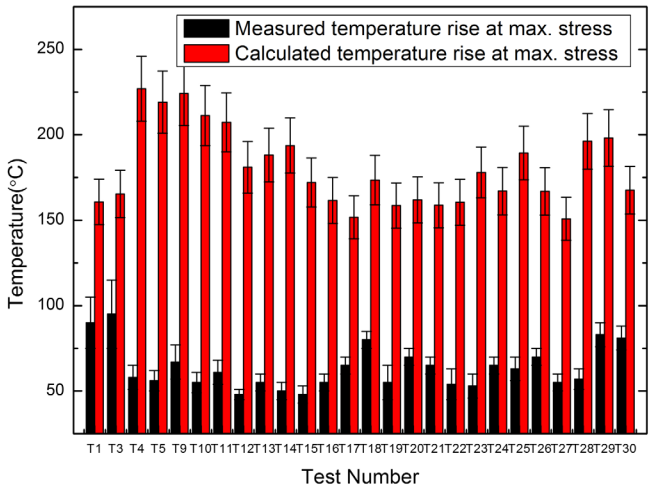

FIG. 3. Summary of the measured and calculated ($\beta = 1.0$) temperature rise at the maximum shear stress for the shear-compression tests.

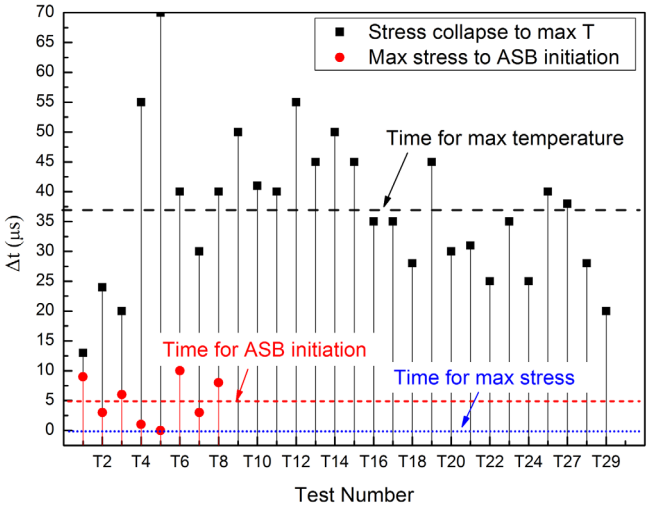

FIG. 4. Time sequence of the occurrence of typical events in the dynamic shear failure process. It shows that peak shear stress comes first, followed by ASB initiation, and the maximum temperature rise comes last. These results greatly clarified the causality of these important events during dynamic loading of the shear-compression specimen.

shear localization is identified by examining the discontinuity of the strips or the grid lines. It should be pointed out that no visible discontinuity of the strips (or ASB) was observed at the maximum stress, which indicates that ASB should initiate *after* the peak stress.

Temperature rise before shear localization.—The temperature rise was measured before and after intense shear localization, as shown in Fig. 1. Similar to previous studies [41], there is hardly any detectable temperature rise at the initial stage of plastic deformation and apparent temperature rise is only observed *after* the maximum shear stress. We summarized in Fig. 3 the temperature rise at the maximum shear stress, i.e., before ASB initiation. All of the temperature rises are in the range of 50 °C–90 °C with acceptable errors. Since this temperature rise is measured before ASB formation, it is relatively uniform at the site of measurement and could be used to derive the Taylor-Quinney factor β [42]:

$$\Delta T = \frac{\beta W_P}{\rho c_V}, \tag{1}$$

where β is the Taylor-Quiney factor and W_P the specific plastic work.

Our results indicate that the Taylor-Quinney factor is between 0.25 and 0.55, and is dependent on the loading rate. This experimental value is far below the traditionally used empirical value of 0.9–1.0. The same tendency was also found by Zhang *et al.* [30], where they derived β values to be from 0.3 at strain rate of 1100/ sec to 0.96 at 4200/ sec for 7075 aluminum alloy.

Temperature within ASB.—Because the size of one pixel for the IR detector corresponds to 150×150 μm, it is larger than the width of the ASB in the titanium specimen used here (about 8 μm). Since the magnification of the optical system is 1:1, the ASB takes up only part of the pixel, which deviates from the calibration condition. ASB may also overlap with more than one pixel. Based on thermal equilibrium, the reading of temperature of the ith pixel could be written as [33]:

$$A_i T_i^4 = A_{hi} T_{hi}^4 + A_{ci} T_{ci}^4 \tag{2}$$

where A_i, A_{hi}, and A_{ci} correspond to the ith, "hot" and "cold" regions of the pixel, respectively. T_i, T_{hi}, and T_{ci} are the overall temperature, the temperature of the hot region (ASB), and the temperature of the cold region, respectively. Based on the measured data of different pixels, the local temperature of ASB is derived to be about 350 °C–650 °C.

Roles of ASB, temperature, and load bearing capacity in the deformation process.—The correlation between ASB initiation, temperature rise, and stress collapse in the deformation of a viscoplastic solid has long been an issue of debate. Thermal softening was believed to be the dominant mechanism that triggers ASB; however, initiation of ASB *at* the maximum stress was the basic assumption of most popular analytical criterions derived by Culver [12], Bai [43], and others as reviewed and summarized by Walley [44]. In other words, the causality has remained unclarified primarily because these processes are temporally very close to each other.

In this Letter, the relative time of ASB initiation, maximum stress, and maximum temperature are recorded by synchronizing high-speed photography, SHPB acquisition system, and IR temperature measurement. A summary of their time sequences is provided in Fig. 4. Combining the experimental results of Figs. 1, 2, and 4, it is clear that ASB initiates *after* the maximum shear stress. This experimental evidence

indicates that the predicted critical shear strain from the above-mentioned criterions might be an underestimate. This observation also suggests that ASB may not be the predominant reason for stress collapse. On the contrary, it might be the stress drop that causes ASB initiation. As for the reason for stress drop (or ASB initiation), there are two potential candidates: thermal softening and microdamage induced by a large strain. From the temperature measurement results, as shown in Fig. 3, the temperature rise at the maximum stress is about 50 °C − 90 °C, corresponding to a stress drop of 30–54 MPa for titanium [23,45]. This thermal softening is global, uniformly distributed over the deformation zone, and is relatively small compared to the overall flow stress. Moreover, the local strain rate begins to increase with the localization process and the strengthening due to strain rate hardening is in the range of 50–60 MPa [23,45]. These considerations suggest that thermal softening alone may not be enough to trigger the sudden stress drop or ASB initiation. Dodd and Atkins [46] found that the softening effect of microvoids in the shear localization process was significant. Xu *et al.* [47] also believed that the sharp drop in the load-carrying capacity was associated with the growth and coalescence of microcracks rather than the occurrence of the shear localization. Microcracks have also been observed in this work during ASB formation by interrupted dynamic tests. Therefore, microdamage induced by the large plastic strain could be another origin of softening. Recently, geometric variation and microstructure inhomogeneity were introduced by Guo *et al.* [48] and Rittel and co-workers [49,50] into their numerical models, where grain rotation and dynamic recrystallization were claimed to be the softening mechanisms, respectively. Nevertheless, the localization process would accelerate the growth of the microcracks, speeding up the temperature rise as well as exacerbating the geometric softening.

The maximum temperature rise was detected about 30 μs after ASB initiation. As such, it is believed that the accelerated temperature rises as detected by the IR sensors are a consequence of the formation and propagation of ASB. By analyzing the high-speed photographic snapshots, this research found that it needs only less than 10 μs for the shear band to propagate through the entire specimen, indicating that the completion of ASB is not necessarily connected to the maximum temperature. Further localized deformation promotes the development of ASB, which in turn leads to further local rises in temperature. In fact, from the experimental results of Duffy *et al.* [34,35], Ranc *et al.* [36], and Rittel *et al.* [41], the delay of temperature rises with respect to stress collapse was observed in materials such as magnesium alloys, titanium alloys, and steels. These tests incorporated direct observation of ASB formation, which makes their causality relationship more explicit. If these events are ranked chronologically, it should be stress peak, ASB initiation, ASB propagation or temperature rise, and maximum temperature or macrocrack formation. The observed fact that temperature rise happens quite after ASB initiation suggests that it should not be the trigger for ASB formation. Therefore, the analytical and numerical analyses found in the literature based on thermal perturbation or thermal softening lose their foundation. Although this conclusion is drawn based on a crystalline material, it should be relevant to amorphous metals where the causality of shear banding has also been an issue of debate. Each of the two major hypotheses, i.e., thermal softening and free volume softening, has its own arguments. Some researchers [51] proposed based on numerical modeling that the onset of shear band was mainly induced by free volume and the temperature increase was its consequence, a notion in line with our experimental observations. As such, we believe that softening from microstructural variation should be equally true for both amorphous and crystalline metals.

To summarize, adiabatic shear localization is traditionally considered to be a thermal-mechanical process, where thermal perturbation or softening is always adopted as the trigger for ASB initiation. Our experimental results unequivocally revealed the opposite. That is, temperature rise occurs *after* ASB formation, indicating that it should be the consequence of ASB rather than its cause. Therefore, the analytical and numerical analyses based on thermal perturbation or thermal softening should be reconsidered. This discovery should lay the foundation for further physical, mechanistic, and mathematic considerations of ASB, a very important phenomenon of instability of many condensed matter systems.

Y. G. and Y. L. would like to thank the financial support by National Natural Science Foundation of China (NSFC Contracts No. 11472227, No. 11672354, and No. 11527803) and the 111 Project (Contract No. B07050). H. C. and S. Z. acknowledge the financial support from NSFC (No. 11802029) and the State Key Laboratory of Explosion Science and Technology (ZDKT18-03).

*Corresponding author.
chenhs@bit.edu.cn
†Corresponding author.
liyulong@nwpu.edu.cn
‡Corresponding author.
fangdn@bit.edu.cn

[1] Y. L. Bai and B. Dodd, *Adiabatic Shear Localization, Occurrence, Theories and Applications* (Pergamon Press, Oxford, New York, Seoul, Tokyo, 1992).
[2] T. W. Wright, *The Physics and Mathematics of Adiabatic Shear Bands* (Cambridge University Press, Cambridge, New York, Port Melbourne, Madrid, Cape Town, 2002).
[3] C. Zener and J. H. Hollomon, J. Appl. Phys. **15**, 22 (1944).
[4] Y. L. Bai, J. Mech. Phys. Solids **30**, 195 (1982).
[5] R. J. Clifton, J. Duffy, and K. A. Hartley, Scr. Metall. **18**, 443 (1984).
[6] T. W. Wright and R. C. Batra, Int. J. Plast. **1**, 205 (1985).

[7] A. Molinari and R. J. Clifton, J. Appl. Mech. Trans. ASME **54**, 806 (1987).
[8] T. W. Wright and J. W. Walter, J. Mech. Phys. Solids **35**, 701 (1987).
[9] R. C. Batra and C. H. Kim, Int. J. Plast. **6**, 127 (1990).
[10] J. W. Walter, Int. J. Plast. **8**, 657 (1992).
[11] T. W. Wright, Int. J. Plast. **8**, 583 (1992).
[12] R. S. Culver, in *Metallurgical Effects at High Strain Rates*, edited by R. W. Rohde *et al.* (Plenum Press, New York, 1973), p. 519.
[13] M. T. Pérez-Prado, J. A. Hines, and K. S. Vecchio, Acta Mater. **49**, 2905 (2001).
[14] M. A. Meyers, Y. B. Xu, Q. Xue, M. T. Perez-Prado, and T. R. McNelley, Acta Mater. **51**, 1307 (2003).
[15] D. R. Chichili, K. T. Ramesh, and K. J. Hemker, J. Mech. Phys. Solids **52**, 1889 (2004).
[16] Y. Yang and B. F. Wang, Mater. Lett. **60**, 2198 (2006).
[17] Y. B. Xu, J. H. Zhang, Y. L. Bai, and M. A. Meyers, Metall. Mater. Trans. A **39A**, 811 (2008).
[18] E. K. Cerreta, J. F. Bingert, G. T. Gray Iii, C. P. Trujillo, M. F. Lopez, C. A. Bronkhorst, and B. L. Hansen, Int. J. Plast. **40**, 23 (2013).
[19] D. Rittel, L. H. Zhang, and S. Osovski, Phys. Rev. Applied **7**, 044012 (2017).
[20] Q. Wei, D. Jia, K. T. Ramesh, and E. Ma, Appl. Phys. Lett. **81**, 1240 (2002).
[21] T. Suo, Y. Chen, Y. Li, C. Wang, and X. Fan, Mater. Sci. Eng. A **560**, 545 (2013).
[22] J. Li, Y. Li, C. Huang, T. Suo, and Q. Wei, Acta Mater. **141**, 163 (2017).
[23] Y. Z. Guo, X. Y. Sun, Q. Wei, and Y. L. Li, Mech. Mater. **115**, 22 (2017).
[24] U. Andrade, M. A. Meyers, K. S. Vecchio, and A. H. Chokshi, Acta Metall. Mater. **42**, 3183 (1994).
[25] J. A. Hines and K. S. Vecchio, Acta Mater. **45**, 635 (1997).
[26] S. Nemat-Nasser, J. B. Isaacs, and M. Liu, Acta Mater. **46**, 1307 (1998).
[27] Q. Wei, T. Jiao, S. N. Mathaudhu, E. Ma, K. T. Hartwig, and K. T. Ramesh, Mater. Sci. Eng. A **358**, 266 (2003).
[28] Y. P. Zheng, W. D. Zeng, Y. B. Wang, D. D. Zhou, and X. X. Gao, J. Alloys Compd. **708**, 84 (2017).
[29] D. Rittel, L. H. Zhang, and S. Osovski, J. Mech. Phys. Solids **107**, 96 (2017).
[30] T. Zhang, Z.-R. Guo, F.-P. Yuan, and H.-S. Zhang, Acta Mech. Sin. **34**, 327 (2017).
[31] L. S. Costin, E. E. Crisman, R. H. Hawley, and J. Duffy, in *Second Conference on the Mechanical Properties of Materials at High Rates of Strain*, edited by H. J. London (The Institute of Physics, Bristol and London, 1979), p. 90.
[32] K. A. Hartley, J. Duffy, and R. H. Hawley, J. Mech. Phys. Solids **35**, 283 (1987).
[33] A. Marchand and J. Duffy, J. Mech. Phys. Solids **36**, 251 (1988).
[34] J. Duffy and Y. C. Chi, Mater. Sci. Eng. A **157**, 195 (1992).
[35] S.-c. Liao and J. Duffy, J. Mech. Phys. Solids **46**, 2201 (1998).
[36] N. Ranc, L. Taravella, V. Pina, and P. Herve, Mech. Mater. **40**, 255 (2008).
[37] D. Rittel, P. Landau, and A. Venkert, Phys. Rev. Lett. **101**, 165501 (2008).
[38] D. Rittel, Z. G. Wang, and M. Merzer, Phys. Rev. Lett. **96**, 075502 (2006).
[39] W. W. Chen and B. Song, *Split Hopkinson (Kolsky) Bar: Design, Testing and Applications* (Springer Science & Business Media, 2010).
[40] D. Rittel, S. Lee, and G. Ravichandran, Exp. Mech. **42**, 58 (2002).
[41] D. Rittel and Z. G. Wang, Mech. Mater. **40**, 629 (2008).
[42] G. I. Taylor and H. Quinney, Proc. R. Soc. A **143**, 307 (1934).
[43] Y. Bai, Res. Mech. **31**, 133 (1990).
[44] S. M. Walley, Metall. Mater. Trans. A **38**, 2629 (2007).
[45] X. Sun, Y. Guo, Q. Wei, Y. Li, and S. Zhang, Mater. Sci. Eng. A **669**, 226 (2016).
[46] B. Dodd and A. G. Atkins, Acta Metall. **31**, 9 (1983).
[47] Y. B. Xu, Y. L. Bai, Q. Xue, and L. T. Shen, Acta Mater. **44**, 1917 (1996).
[48] Y. Z. Guo, Y. L. Li, Z. Pan, F. H. Zhou, and Q. Wei, Mech. Mater. **42**, 1020 (2010).
[49] J. A. Rodríguez-Martínez, G. Vadillo, D. Rittel, R. Zaera, and J. Fernández-Sáez, Mech. Mater. **81**, 41 (2015).
[50] D. Rittel, Z. G. Wang, and A. Dorogoy, Int. J. Impact Eng. **35**, 1280 (2008).
[51] M. Q. Jiang and L. H. Dai, J. Mech. Phys. Solids **57**, 1267 (2009).